MAX-PLANCK-GESELLSCHAFT

Journal of Catalysis 218 (2003) 365-374.

AC FHI

Isomerization of *n*-Butane and of *n*-Pentane in the Presence of Sulfated Zirconia: Formation of Surface Deposits Investigated by In Situ UV–vis Diffuse Reflectance Spectroscopy

Rafat Ahmad, Jörg Melsheimer, Friederike C. Jentoft, and Robert Schlögl*

Department of Inorganic Chemistry, Fritz Haber Institute of the Max Planck Society,

Faradayweg 4-6, 14195 Berlin, Germany

Abstract: Catalytic performance and formation of carbonaceous deposits were studied simultaneously during alkane isomerization over sulfated zirconia in a fixed bed flow reactor with an optical window for in situ UV–vis diffuse reflectance spectroscopy. The reactions of *n*-butane (5 kPa) at 358 and 378 K and of *n*-pentane (0.25 kPa) at 298 and 308 K passed within 5 h or less through an induction period, a conversion maximum, and a period of deactivation; a steady activity of 41 and 47 μmol g^{-1} h^{-1} (isobutane formation) and ≈2.5 μmol g^{-1} h^{-1} (isopentane, both temperatures) remained. UV–vis spectra indicate the formation of unsaturated surface deposits; the band positions at 310 nm (*n*-butane reaction) and 330 nm (*n*-pentane) are within the range of monoenic allylic cations. More highly conjugated allylic cations (bands at 370 and 430 nm) became evident during *n*-butane reaction at 523 K. The chronology of events suggests that the surface deposits are (i) a result only of the bimolecular and not the monomolecular reaction mechanism, and (ii) are formed in a competitive reaction to the alkane products.

Keywords: *n*-butane, *n*-pentane, isomerization, sulfated zirconia, deactivation, in situ UV–vis spectroscopy

*corresponding author, email: jentoft@fhi-berlin.mpg.de

1. Introduction

The skeletal isomerization of alkanes plays an important role in petroleum processing, leading to a demand for solid catalysts that are active at low temperatures where the desired branched hydrocarbons are thermodynamically favored. Sulfated zirconia (SZ) materials are active for the conversion of *n*-butane into isobutane at 373 K (1). Unfortunately, the isomerization activity declines rapidly (2) unless special measures are taken. Several suggestions have been made in order to explain the deactivation process, among them: 1- Formation of hydrocarbon surface deposits ("coke") (2-11), 2- surface reduction ($Zr^{4+} \rightarrow Zr^{3+}$) by the reacting hydrocarbon (4), 3- reduction of the surface sulfate groups and H_2S formation (5), 4- change in the surface phase of zirconia from tetragonal to monoclinic (12), and 5- surface poisoning by water (7). Evidence for these hypotheses mainly arises from investigations of the fully or partially deactivated catalyst (2-4,7-12), often after removal from the reactor. A true in situ experiment, i.e. a continuous monitoring of the catalyst surface during the reaction and a correlation of surface properties with the actual catalytic activity is lacking.

Diffuse reflectance spectroscopy in the ultraviolet and visible region is a suitable technique for studying electronic transitions of heterogeneous catalysts (13-18). Additionally, the technique is potentially very sensitive for the detection of adsorbed reaction intermediates or side products, depending on the chromophores present in these species. Particularly useful is the combination of spectral information with simultaneously acquired catalytic data. So far, sulfated zirconia has only been investigated by UV–vis spectroscopy in a deactivated state, i.e. ex situ after *n*-butane isomerization (8,9). Chen et al. (9) assigned a band at 292 nm to allylic cations; Spielbauer et al. (8) attributed three bands at 306, 366, and 400 nm to allylic cations, polyenylic cations, and polycyclic aromatic compounds, respectively. Unsaturated species are obviously formed at some point during the interaction of *n*-butane or its reaction products with the surface; and the UV–vis spectra of a number of cationic hydrocarbon species in solution (19,20) or on zeolite surfaces (21,22) are available in the literature and can be used for interpretation.

In principle, alkane isomerization can proceed through two different pathways, a bimolecular

mechanism involving an alkylation and a scission step or a monomolecular mechanism (intramolecular rearrangement). Side products of the bimolecular mechanism of C_n-alkane isomerization are disproportionation products, i.e. C_{n-1} and C_{n+1} alkanes. Monomolecular isomerization is easily possible for C_n hydrocarbons with $n \geq 5$ (23), for shorter hydrocarbons the intramolecular rearrangement was believed unfavorable because of the temporary formation of a primary carbenium ion. However, according to recent results, *n*-butane isomerizes not only through a bimolecular pathway involving the formation of a C_8 intermediate, which is indicated by the appearance of C_3- and C_5-alkanes as side products, but also through a monomolecular mechanism (24). Unfortunately, the maximum rates for all products coincide at the same time on stream under typical reaction conditions (25). In the case of *n*-pentane isomerization catalyzed by sulfated zirconia materials, it is possible to identify predominance of the monomolecular or the bimolecular pathway because the isopentane and isobutane production rates reach their maxima at different times on stream (26,27). Using *n*-pentane as a reactant thus offers the opportunity to reveal whether deactivation is solely connected to one or the other pathway.

The aim of this work is to investigate the evolution of surface species on sulfated zirconia during *n*-butane and *n*-pentane isomerization by in situ UV–vis spectroscopy, and to find correlations between catalytic activity and the nature and concentration of adsorbates.

2. Experimental

2.1. In situ UV–vis spectroscopy

The equipment, a modified Perkin–Elmer Lambda 9 spectrometer equipped with an integrating sphere and a microreactor cell (in-house design), is described in detail in reference (28). The horizontally mounted microreactor consists of an inner tube (ID: 15 mm, OD: 20 mm) with a circular frit 2.8 mm from the end to accommodate the powder bed. The inner tube is enclosed by an outer tube (ID: 21 mm, OD: 25 mm) whose circular optical quartz window (Suprasil®, Heraeus) holds the powder bed in place. The volume between window and frit is thus fixed; it holds about 1.2 g of the SZ catalyst. The reactor is placed in a tubular oven with the reactor window at a distance of 12 mm from the integrating sphere; this distance is

bridged by a ceramic tube of high reflectivity and low thermal conductivity (MACOR®, Kager). The temperature is measured with a thermocouple at the catalyst-free side of the frit, i.e. upstream from the bed and towards the center of the oven.

All spectroscopic measurements were carried out sequentially over the range of 250–860 nm with a scan speed of 240 nm min^{-1}, a nominal slit width of 5.0 nm (equivalent to a resolution of 5.06–4.20 nm in the range 200–800 nm), a response time of 0.5 s, and a step width of 1 nm. Spectralon® was used as the white standard in the reference position.

2.2 Sample preparation and reaction conditions

Sulfated zirconium hydroxide XZO 682/1 from MEL Chemicals was calcined in portions of 10 g (29) in a 200 ml min^{-1} flow of synthetic air for 3 h at 823 K to produce sulfated ZrO_2. The SO_3 content of the precursor is 5-6 wt% SO_3 according to the information supplied by the manufacturer. After calcination, thermogravimetric experiments showed a weight loss corresponding to 4.7 wt% SO_3. The surface area of the calcined material was determined by five-point-BET to 83 m^2 g^{-1}. The calcined catalyst (1.24–1.31 g) was loaded into the cell and heated in 65 ml min^{-1} helium flow to 723 K with a heating rate of 5 K min^{-1}. The catalyst sample was held at 723 K for 1.5 h, during this time the gas flow was switched to 30 ml min^{-1} of pure O_2. The sample was then cooled to room temperature and reheated to the reaction temperature in helium. Reaction temperatures were 358, 378, 423, and 523 K for *n*-butane, and 298 and 308 K for *n*-pentane. The reaction was carried out at atmospheric pressure, using a 50 ml min^{-1} flow. Analysis of the gas phase products was performed by on-line gas chromatography (Varian 3800) using flame ionization detection. With the selected temperature program, the PoraPLOT Q column (Chrompack) allowed the separation of all alkanes/alkenes and their respective isomers up to C_6 in one run. The detection limits were about 1 vpm for C_5 and C_4 hydrocarbons, about 2 vpm for propane, and about 5 vpm for methane. The detection limits for some alkene isomers in the presence of the respective alkanes were higher, because the setup was optimized for fast iso-/*n*-alkane separation and not for complete alkene/alkane isomer separation. Butane (Linde, 3.5) was fed as a 5.0 vol % *n*-butane in helium mixture, which contained 21 vpm isobutane as impurity. Following the supplier's specification and accounting for the dilution, the sum of impurities originating

from the "*n*-butane" such as e.g. isobutane and butenes should not exceed 25 vpm in the mixture. Pentane (Linde, 2.0) was fed as a 0.25 vol % *n*-pentane in helium mixture, which contained 4 vpm isopentane and 2 vpm *n*-butane as impurities. No other impurities were detected in the two feed mixtures, and the impurities were accounted for in the following calculations.

Conversion to gas phase products is defined as 100 x (∑ concentrations of individual gas phase products)/(alkane concentration in the feed). Yield is defined as 100 x (concentration of individual gas phase product)/(alkane concentration in the feed). Selectivity is defined as 100 x yield/(conversion to gas phase products). Carbon loss expressed in % is defined as 100 x (concentration of *n*-alkane in feed x number of carbon atoms of the *n*-alkane - ∑ concentrations of individual products x number of carbon atoms in product molecule)/(concentration of *n*-alkane in feed x number of carbon atoms of the *n*-alkane). The rate of carbon loss expressed in moles C_5 is defined as (moles of *n*-alkane fed per h per g catalyst x number of carbon atoms of the *n*-alkane - ∑ moles of individual products formed per h per g x number of carbon atoms in product molecule)/5.

3. Results

3.1 Reaction of *n*-butane and *n*-pentane

The products of *n*-butane reaction were isobutane, propane, isopentane, and *n*-pentane at 358, 378, and 423 K, and additionally methane, ethane, and ethene at 523 K. At 358 K, an induction period of 120 min was observed before the conversion increased significantly. A maximum in conversion was reached after 172 min at 358 K and after 47 min at 378 K; afterwards the conversion declined steadily. At 423 and 523 K, no induction period was detected, i.e. the conversion declined more or less from the beginning. The conversion to gas phase products increased with temperature and the highest values ranged from 5 % (358 K) to 32 % (523 K). Carbon loss was sometimes observed on the first few data points and ranged from 5–15% without a clear trend with temperature. At 358, 378, and 423 K, the selectivity to isobutane passed through a minimum as the conversion to gas phase products and the propane selectivity passed through a maximum. The selectivity to isobutane at this minimum ranged

from 90 % at 423 K to 94 % at 358 K. An isobutane selectivity < 90% was observed for the first hour at 523 K. A steady state was reached after about 5 h on stream, the rates of isobutane formation were then 41 (358 K), 47 (378 K), 156 (423 K), and 233 (523 K) μmol g^{-1} h^{-1}. The yield of isobutane from reaction of *n*-butane as a function of time on stream at 358, 378, 423, and 523 K is shown in Figure 1.

The detectable products of *n*-pentane reaction were isobutane, isopentane, *n*-butane, propane, *n*-hexane, 2-methylpentane, and 3-methylpentane. The conversion to gas phase products increased with time on stream and reached its maximum at 21 % after 96 min at 298 K and at 26 % after 80 min at 308 K before it declined rapidly. The carbon balance indicated losses as high as 20-40 % in the first 50 min for both temperatures. The selectivities to isopentane at maximum isopentane formation rate were 37 % at 298 K and 23 % at 308 K. The rate of isopentane formation after 5 h on stream was ≈2.5 μmol g^{-1} h^{-1} for both reaction temperatures, 298 K and 308 K. The yields of various gas phase products from reaction of *n*-pentane as a function of time on stream at 308 K are shown in Figure 2.

3.2 In situ UV–vis spectroscopy

The original data represent the reflectance of the sample with respect to the reference material, which was Spectralon®. In Figure 3, the UV–vis spectrum of activated sulfated zirconia is shown in units of reflectance. In the range 400–800 nm, the material is highly reflecting without any specific absorptions. Below 400 nm, a strong decrease of the reflectance is observed; the band gap is, according to the not very consistent literature, expected towards shorter wavelengths, i.e. between 250 and 285 nm (30-32).

Any spectra taken after contact with the reactants will represent absorptions arising from (i) changes to the sulfated zirconia and from (ii) surface deposits. If surface deposits are chemisorbed changes will be inflicted to the surface structure but they may not be detectable by UV–vis spectroscopy. If the sulfated zirconia does not change during the reaction, the system could be regarded as the simple case of an organic material adsorbed on the surface of a diluent (=sulfated zirconia). Such systems have been analyzed and discussed by Kortüm (33). As long as the organic material is in a molecular-disperse state and its concentration is

low with a molar fraction of 10^{-3} or less, the Kubelka-Munk function is proportional to the concentration. Absorption of the diluent can be eliminated by making two measurements, one of the diluent vs. a white standard (sulfated zirconia vs. Spectralon®) and one of the mixture of diluent plus organic material vs. the white standard (sulfated zirconia + alkane vs. Spectralon®), and then calculating the difference. However, Kortüm's discussions refer to strongly absorbing organic material adsorbed on a weakly absorbing diluent. The analysis thus appears suitable for the range > 400 nm, but not a priori for the range of strong absorption by the catalyst. Application of the Kubelka-Munk function is usually limited to systems with diluted absorption sites, which e.g. is not the case for the band gap transition.

The dashed line in Figure 3 shows the spectrum of sulfated zirconia after 14 h on stream for *n*-butane reaction at 423 K in units of reflectance. The difference between the spectrum after activation and the spectrum after reaction, i.e. R_{sz} - $R_{sz+alkane}$ is also displayed. Assuming no changes to the sulfated zirconia, the difference spectrum suggests the presence of a band at about 310 nm. The band position shifts to 303 nm if not the simple difference spectrum but the difference between the Kubelka-Munk functions is calculated. A discrepancy in the position depending on the method of analysis (1- position from original spectrum in reflectance or Kubelka-Munk units, 2- difference of reflectance spectra, 3- difference of Kubelka-Munk representations) also resulted for other bands that overlapped with the strong absorption by the catalyst. In the comparison of and with literature data this effect has to be accounted for.

In order to see the development of the changes but to avoid overinterpretation of the data at the current state of investigation, all data are presented as simple difference spectra in the following (Figures 4-6), and it is understood that these differences include possible changes of the sulfated zirconia. The difference spectra taken at low temperatures were noisy and exact determination of band position and height was not always possible. For experiments with different catalyst batches under identical conditions the positions did not differ by more than 5 nm. For estimation of band intensities as a function of time on stream, band areas were evaluated.

Figure 4 shows a series of spectra obtained during the reaction of *n*-butane at 378 K. A weak

band with a maximum at about 310 nm developed with increasing time on stream. A band at this position was observed at all four reaction temperatures. It was always the first band that evolved; specifically it was detected after about 150 min at 358 K, after 24 min at 378 K, after about 10 min at 423 K, and from the beginning at 523 K. At 358, 378, and 423 K the band at 310 nm remained the only detectable band within the observation span of 6 h. The intensity of this band approached a constant level at all temperatures. At 523 K, two further bands appeared in the spectrum with increasing time on stream as shown in Figure 5; first a band at 370 nm after 20 min on stream and then a band at 430 nm after 6 h. These two bands continued growing within the observation span of 15 h.

Figure 6 shows a series of spectra obtained during the reaction of *n*-pentane at 298 K. The spectra were characterized by a broad feature (FWHM ≈ 60 nm after 798 min) with a maximum at 330 nm, which grew in intensity with increasing time on stream. Under all applied conditions, the feature at 330 nm always developed, but no other bands were detected within the observation span of at least 6 h.

4. Discussion

4.1 Band assignments

n-Butane isomerization: Chen et al. (9) and Spielbauer et al. (8) investigated sulfated zirconia that had been deactivated during *n*-butane isomerization and found bands at 292 nm (position from original spectrum, measured in reflectance (9)) and 306 nm (difference of reflectance spectra (8)), which they attributed to allylic species. Förster et al. (21) studied the interaction of a number of C_3 compounds with zeolites and reported band positions between 310 and 345 nm (spectra corrected for the background absorption of the zeolite, measured in transmission) for monoenic allylic cations. Pazé et al. (22) exposed H-Ferrierite to 1-butene and obtained bands at 1580 cm^{-1} and at 310 nm (original spectrum, measured in reflectance), which were ascribed to a monoenic allylic cation. Their assignment was based on literature data of ions on zeolite surfaces (21) and in solution (19,20) and the fact that the band at 310 nm partially disappeared upon exposure to NH_3, which is presumed to neutralize positive charges. Accordingly, the pronounced band at 310 nm that forms during *n*-butane isomerization

(Figures 3-5) in our experiments may also be attributed to the π-π^* transition of allylic cations. Alkyl groups as substituents cause a shift of typically +5 nm (34), which is not enough to properly identify the chain length of our allylic species. The asymmetric shape of the band suggests that possibly several species contribute; such species could be of different chain length or just structural isomers. As the ratio of propane to pentanes in the effluent stream is always larger than one, C_5-species will have to remain on the surface if the sole origin of propane is the disproportionation of a C_8-intermediate. The presence of C_5-species on the surface thus seems likely, and is further corroborated by the spectra obtained at 523 K. Namely, the bands at longer wavelengths can be attributed to allylic cations with conjugated double bonds, whose formation requires a hydrocarbon backbone of a certain minimum length. Specifically, the bands at 370 and 430 nm are identified as dienic and trienic allylic cations (21,22); for such ions, a chain length of at least 5 or 7 carbon atoms, respectively, is required. The assignment is deduced from the work of Pazé (22) who assigned bands at 370 and 435 nm to dienic and trienic ions, and from the work of Förster (21) who assigned bands at 370–390 nm to dienic and at 430–480 nm to trienic allylic cations, and suggested that initially formed monoenic species transform to more highly conjugated species. Spielbauer et al. (8) have also attributed a band at 366 nm formed during *n*-butane isomerization at 523 K on sulfated zirconia to "polyenylic" cations; a band at 410 nm formed at 473 K in the presence of H_2 in the feed was attributed to polycyclic aromatic compounds. The band positions are in principle too unspecific to exclude the presence of aromatic species on our samples; however, the positions match the data reported for dienic and trienic allylic cations extremely well. The extinction coefficients of allylic cations are in the order of magnitude of 10^4 l mol^{-1} cm^{-1} (19); and as with polyenes, the coefficients should increase with conjugation (up to a factor of 2 per additional double band (34)). The spectra could thus be deceiving with respect to the amount of dienic and trienic allylic cations on the surface.

n-Pentane isomerization: The broad feature at 330 nm observed during the reaction of *n*-pentane (Figure 6) also falls within the range for absorptions attributable to allylic cations. In the *n*-pentane reaction, the rate of formation of isobutane is throughout the entire run more than one order of magnitude larger than the sum of rates of formation of hexane isomers

(factor of 25–40 at 298 K and 19–65 at 308 K); actually more isobutane than isopentane is produced within the observation span. If isobutane is formed through disproportionation of C_{10} intermediates, C_6 hydrocarbons will have to remain on the surface. The width of the feature suggests that it is a superposition of several single bands, possibly different C_6 isomers. Alternatively, the band could be assigned to cyclopentenyl cations, which were proposed as causes of deactivation by Luzgin et al. (35), who monitored the isomerization of *n*-pentane at room temperature by ^{13}C-MAS-NMR. Bands of more highly conjugated species were not detected; both, our observations with the *n*-butane reaction and Pazé's (22) results suggest that the reaction temperature (max. 308 K in our case) is not high enough for the formation of such species. At a low enough reaction temperature the formation of polyunsaturated deposits can apparently be avoided, for *n*-butane as well as for *n*-pentane reaction.

4.2 Course of events during the reaction of *n*-butane

Evolution of the band at 310 nm with time during n-butane isomerization at 358 K and 378 K (Figure 7): In the first 120 min at 358 K, the catalyst produces isobutane with high selectivity, but no bands evolve in the UV–vis region. Either there are indeed no surface species, or they are too few to be detected or too short-lived, or they do not absorb within the UV–vis region. Species such as carbenium ions, if formed from adsorbing alkanes, would not be visible in our spectra because they do not absorb above 210 nm (20), nor would alkanes themselves be detectable. Whatever triggers the sudden increase in conversion – changes to the catalyst or accumulation of surface species – is not detectable in the UV–vis spectra. One possibility is that the reaction initially proceeds through a monomolecular mechanism, and only as (i) enough branched species are available on the surface and/or (ii) alkenes have been formed, alkylation to give C_8 species (bimolecular mechanism) can take place. The accumulation of contaminant butenes from the feed stream as a reason for the induction phase appears unlikely, because the length of the induction period at constant feed flow is a function of temperature (see Figure 1) and the initial isomerization activity is almost independent of the alkene concentration in the feed stream (10), although there is a significant influence of the alkene concentration on the overall reaction profile (10, 36). Traces of propane in the product

stream throughout the entire reaction profile indicate that the reaction never proceeds exclusively through the monomolecular isomerization mechanism. Significant amounts of propane and pentanes, which indicate the formation of C_8 species, are detected only at high conversions; they could thus be secondary products. However, Cheung et al. (25) stated that propane and pentanes are apparently primary products of the reaction of *n*-butane in the presence of Fe- and Mn-promoted sulfated zirconia. Also, cracking of C_8 hydrocarbons preferentially produces C_4 species rather than C_3 and C_5 species (23), i.e. propane and pentanes are always formed in small quantities and may, as in our case the pentanes, only become detectable at high conversions. The isobutane selectivity, which during the peak activity drops from 97 to 94 % at 358 K and from 94 to 91 % at 378 K and then rises again to 99 % at 358 K and to 98 % at 378 K, is the best indicator for an increased contribution of the bimolecular mechanism to product formation during the period of high activity. Because the rate of formation of propane was always larger than the sum of rates of formation of *n*- and isopentane under the selected conditions, C_5 species must be retained at the surface. It can of course not be excluded that a C_3 species remains on the surface as a C_5 species desorbs, and equally, one out of two C_4 species may remain on the surface. More generally speaking, if a C_8 intermediate cleaves into a neutral and a charged species (e.g. alkene/alkane + cation), the charged species will – for the time being – remain on the surface.

During the period of increasing conversion, unsaturated surface species are formed. In Fig. 7, the evolution of the band at 310 nm, attributable to allylic cations, with time on stream is shown together with the rates of formation of isobutane and propane (indicative of disproportionation). The increase in conversion at 378 K and the band growth are fairly rapid and it is not possible to decide if one precedes the other. From the data taken at 358 K, it becomes evident that the species absorbing at 310 nm is obviously not an intermediate; the highest conversion is reached before the band is fully developed. The initial, fast increase of the band coincides with the maxima of all rates; the band grows as the rates already decrease. The band appears to be associated with the bimolecular mechanism but the species is obviously not a side product but a competitive product, i.e. the selectivity changes from gas phase product to deposit formation. After the band at 310 nm is saturated, the catalyst

continues to produce isobutane, i.e. there exist active sites that are not affected by the presence of the surface deposits.

For the intensity profile of the 310 nm band with time on stream, specifically for the approach of a constant level, a second explanation is possible. Additional species that absorb at 310 nm could still be formed on the surface; but if the species were not molecularly dispersed, the intensity would no longer increase linearly with concentration. Given the reaction profile with its fast decrease in conversion, the explanation seems unlikely. However, at longer time on stream trienic allylic cations are observed that require at least a C_7 backbone. Such trienic cations could arise from long-lived C_8 surface species that are slowly dehydrogenated but they could also be oligomerization products of shorter chain length species, in which case these species would have to be in close proximity and thus not molecularly dispersed.

Evolution of bands at 310, 370, and 430 nm with time during n-butane isomerization at 523 K (Figure 5): In addition to the band at 310 nm, which grows from the beginning of the reaction, 2 bands at 370 and 430 nm start to grow after 20 min and 6 h on stream. These bands indicate that dienic and trienic allylic cations (21,22) are formed during *n*-butane reaction at 523 K. The intensity of the band at 310 nm does not decrease as the additional bands grow. The species absorbing at 310 nm are thus (i) either formed at the same rate as they are further dehydrogenated to give the more highly unsaturated species, or (ii) they are not intermediates for the dienic and trienic allylic cations, implying that the differently conjugated species are situated on different sites.

There is no change in the rate of formation of isobutane as the 310 nm band saturates, and also not as the band at 430 nm starts to grow. The adsorption sites for these species are thus independent of the sites that produce isobutane. The presence of a triply unsaturated species (430 nm), which requires at least a C_7 backbone, suggests that after 6 h on stream (i) alkylation is still occurring, or long-lived C_7 species are present from earlier stages of the reaction, and (ii) dehydrogenation is favored over cleavage. The fact that new species are formed after so many hours suggests that the catalyst surface and the thereon adsorbed species undergo changes not apparent in UV–vis spectra.

4.3 Course of events during the reaction of *n*-pentane

Evolution of band at 330 nm with time during n-pentane isomerization at 298 K and 308 K (Figures 8 and 9): Similar to the observations during *n*-butane isomerization, there were no bands detectable during the induction period. With *n*-pentane as feed though, a considerable carbon loss (around 40 %) could be detected within the first minutes on stream, and before the catalyst showed any significant activity. The adsorbate does not absorb in the UV–vis range, i.e. within the early stages of the reaction, no significant amounts of unsaturated surface species are present on the surface. The subsequent increase in isopentane production results probably from monomolecular isomerization, because the cracking of a C_{10} species would produce more C_4 than C_5 hydrocarbons (37). Shortly after, isobutane becomes the main product indicating that the bimolecular mechanism predominates. As the production of isobutane becomes significant, the band at 330 nm begins to grow. The sequence of events with time on stream during *n*-pentane isomerization is illustrated in two different ways in Figures 8 and 9. Figure 8 shows the pentane reaction at 308 K, and the band area (band at 330 nm) is plotted; Figure 9 shows the pentane reaction at 298 K, and the first derivative of the band area, i.e. the band growth rate is plotted. The initial carbon loss (expressed in units of C_5), indicating the adsorption of *n*-pentane, can clearly be recognized. As the carbon loss declines from its first maximum, the isopentane formation rate reaches its maximum, followed by the maximum in isobutane formation rate, and finally, band growth at 330 nm. Both figures reveal an increase in carbon loss as the band develops, suggesting that gas phase species are consumed in the process. Figure 8 shows (i) that only as the production of isobutane becomes significant, does the band at 330 nm begin to grow, indicating a relation between bimolecular mechanism and deposit formation and (ii) opposing trends for the formation of saturated gas phase products and unsaturated surface species, indicating that these two reactions are competitive and that dehydrogenation eventually prevails. Figure 9 underlines that the maximum in band growth is reached only after the maxima in product formation.

4.4 Implications for low temperature alkane isomerization in the presence of sulfated zirconia

Based on the reactor effluent gas analysis (Figures 1 and 2), the UV–vis spectroscopic measurements (Figures 3-6), and the correlation of these data (Figures 7-9), the following picture evolves for the catalytic action and deactivation of sulfated zirconia in isomerization of alkanes at low temperature (358 and 378 K for *n*-butane, 298 and 308 K for *n*-pentane):

1. As it must, the reaction starts out with chemisorption of the *n*-alkane. Under the applied conditions, the adsorption was observable as a significant initial carbon loss when *n*-pentane was the reactant. There was no immediate observation of bands in the UV–vis spectra; an initial high carbon loss is thus not equivalent to "coking" of the catalyst. In order to be able to detect conversion and spectral changes, the applied *n*-butane partial pressure was 20 times higher than the *n*-pentane partial pressure; when *n*-butane was the reactant, the small fraction from the stream that was adsorbed could thus not be extracted from the carbon balance.

2. The conversion starts at a low level and then increases slowly (often called "induction period"), and formation of the isomerization product is the predominant reaction for both reactants during this period. For *n*-butane, both, the mono- and the bimolecular mechanism, lead to the same main product, viz. isobutane. For *n*-pentane, the two mechanisms lead to different main products; the monomolecular mechanism produces isopentane, while isobutane is the main scission product from the C_{10} intermediate of the bimolecular mechanism. The product distribution data for *n*-pentane reaction show that isomerization first proceeds through the monomolecular mechanism; for *n*-butane the data are consistent with, but not evidence for a monomolecular mechanism whose supposition is in agreement with the literature. Based on catalytic data, it was previously suggested by Matsuhashi et al. (38) that alkane (*n*-butane and *n*-pentane) isomerization on SZ in the beginning proceeds through a monomolecular mechanism. Luzgin et al. (35) confirmed contribution of the monomolecular mechanism to the *n*-pentane isomerization on SZ by isotopic labeling and NMR spectroscopy. Suzuki and Okuhara (24) proved the contribution of a monomolecular mechanism for *n*-butane on SZ by isotopic labeling and GC-MS, but investigated only how the two mechanisms compete depending on temperature and not depending on time on stream or degree of deactivation.

3. As the conversion increases further and approaches its maximum, unsaturated surface

species are observed by UV–vis spectroscopy. The formation of C_{n-1} and C_{n+1} hydrocarbons as side products (disproportionation) indicates the bimolecular mechanism. For *n*-butane reaction, the bimolecular mechanism appears acceptable in that it still leads predominantly to isobutane. According to Matsuhashi et al. (38) the activation energy for monomolecular isomerization of *n*-butane is 54 kJ mol^{-1} and for bimolecular isomerization is 37 kJ mol^{-1}. A major fraction of the total amount of isobutane produced within the most active stage of the catalyst thus arises from the bimolecular mechanism. Analysis of products in a batch system (with use of ^{13}C-labelled *n*-butane) after a certain time on stream will reflect this situation; e.g. Adeeva et al. (39) concluded that the isomerization proceeded through a bimolecular mechanism, while Suzuki and Okuhara (24) with a more sensitive method of analysis found some contribution of the monomolecular mechanism. For *n*-pentane reaction, the bimolecular mechanism is undesirable because isobutane becomes the main product.

4. As the conversion passes through its maximum, rapid formation of unsaturated surface species, presumably allylic cations, is evidenced by bands at 310 (*n*-butane reaction) and 330 nm (*n*-pentane). The activity is already declining as these bands reach their highest (and final) intensity, indicating that the allylic species are not intermediates of the reaction. The formation of allylic species requires the abstraction of 3 hydrogen atoms from an alkane, e.g. in the form of dihydrogen and hydride. If these species were intermediates, the hydrogen atoms would have to be added again to obtain the saturated products. None of the according bands ever decreases in intensity; under the selected conditions the formation of allylic surface species is thus irreversible. Particularly, the data obtained during *n*-pentane reaction show that the formation of the allylic species is associated with the occurrence of the bimolecular mechanism; there are no unsaturated surface species detected when the isopentane production is its maximum, chronologically before the isobutane formation and thus the bimolecular mechanism prevail. Rather than being consecutive reactions, the formation of the allylic species and the formation of saturated gas phase products are competitive reactions, rooted in a common intermediate.

The selectivity of the catalyst changes such that dehydrogenation is the predominant reaction. The allylic cations block active sites, specifically the sites that promote the fast bimolecular

mechanism, but there are sites remaining that are responsible for the long-term activity. These two types of sites may be identical to the "more active" and "less active" sites in the model of Kim et al. (11) who believe the "less active" sites produce activity at longer times on stream.

5. After the steep drop, the conversion becomes almost stable and the selectivity towards the isomerization product increases (both reactants). The bands at 310 and 330 nm stop growing. There are obviously a sufficient number of sites remaining for the reaction to continue, and the selectivity data suggest that the contribution of the monomolecular mechanism increases. With increasing temperature, the high initial activity in *n*-butane isomerization declines more rapidly and the long-term activity increases (Figure 1); the fraction of isobutane produced via the monomolecular mechanism within the total amount of isobutane formed over a certain time on stream should increase. Consistently, Suzuki and Okuhara (24) in their batch-type experiment find an increasing contribution of the monomolecular mechanism in *n*-butane isomerization with increasing temperature.

5. Summary

The investigation of *n*-butane and *n*-pentane isomerization on sulfated zirconia by in situ UV–vis diffuse reflectance spectroscopy using a fixed-bed flow reactor revealed important information on the nature of surface deposits. For the first time, the formation of such deposits could be related to the catalyst performance and the reaction mechanism.

Literature data and product distributions suggest that alkane isomerization proceeds simultaneously through a monomolecular and a bimolecular mechanism, the latter is indicated through the occurrence of disproportionation byproducts (C_{n-1}, C_{n+1} alkanes). At low reaction temperatures (*n*-butane: 358, 378 K; *n*-pentane: 298, 308 K), conversions were low at the beginning, increased and went through a maximum, and finally declined to a steady level. During the period of maximum activity, propane and pentanes were observed as byproducts in *n*-butane reaction, and isobutane as main product in *n*-pentane reaction, indicating the bimolecular mechanism. During the periods of low activity in the beginning and at long time on stream, the high selectivity to isobutane and to isopentane in the respective reactions indicated contributions of the monomolecular mechanism.

In the course of the reaction, unsaturated species were formed on the surface of sulfated zirconia, characterized by bands at 310 (*n*-butane reaction) and 330 (*n*-pentane) nm. The positions of these bands are consistent with those of monoenic allylic cations. More highly conjugated allylic cations were observed for reaction of *n*-butane at 523 K.

The bands of singly unsaturated species only grew during the period of high conversion. More specifically, the fastest growth was observed in the period of decreasing activity, excluding the species as reaction intermediates. The formation of unsaturated surface deposits is linked to the occurrence of the bimolecular mechanism. The opposing trends in the rates of formation of saturated gas phase products and the formation of allylic cations indicate competitive reactions, possibly connected through a common intermediate.

In summary, in situ UV-vis spectroscopy proved extremely helpful in connecting the formation of surface deposits to catalytic performance and thus to a particular reaction path. With respect to the sulfated zirconia catalyst, maybe more attention should be paid to the low long-term activity than to the short-lived high activity that leads to partial coking of the surface.

Acknowledgements

The authors would like to thank MEL Chemicals for providing the catalyst raw material, A. Broshnik for the BET measurements, and R.E. Jentoft for the TG measurements. The DAAD is acknowledged for granting financial support to R. Ahmad. F.C. Jentoft expresses special thanks to B.C. Gates; some thoughts were initialized by *n*-butane reactor studies conducted during a stay in his group in 1994/95.

References

1. Hino, M., Kobayashi, S., and Arata, K., *J. Am. Chem. Soc.* **101**, 6439 (1979).

2. Li, B., and Gonzalez, R. D., *Appl. Catal. A: General* **174**, 109 (1998).

3. Li, B., and Gonzalez, R. D., *Catal. Today* **46**, 55 (1998).

4. Vera, C. R., Pieck, C. L., Shimizu, K., Querini, C. A., and Parera, J. M., *J. Catal.* **187**, 39 (1999).

5. Li, B., and Gonzalez, R. D., *Appl. Catal. A: General* **165**, 291 (1997).

6. Ng, F. T. T., and Horvát, N., *Appl. Catal. A: General* **123**, 197 (1995).

7. Comelli, R. A., Vera, C. R., and Parera, J. M., *J. Catal.* **151**, 96 (1995).

8. Spielbauer, D., Mekhemer, G. A. H., Bosch, E., and Knözinger, H., *Catal. Lett.* **36**, 59 (1996).

9. Chen, F. R., Coudurier, G., Joly, J.-F., and Védrine, J. C., *J. Catal.* **143**, 616 (1993).

10. Fogash, K. B., Hong, Z., Kobe, J. M., and Dumesic, J. A., *Appl. Catal. A: General* **172**, 107 (1998).

11. Kim, S. Y., Goodwin, J. G. Jr., and Galloway, D., *Catal. Today* **63**, 21 (2000).

12. Li, C., and Stair, P. C., *Catal. Lett.* **36**, 119 (1996).

13. Centi, G., Lopenz Nieto, J., and Iapalucci, C., *Appl. Catal.* **46**, 197 (1989).

14. Timofeeva, N. N., Demidov, A. V., Davydov, A. A., and Kozhevnikov, I. V., *J. Mol. Catal.* **79**, 21 (1993).

15. Melsheimer, J., Mahmoud, S. S., Mestl, G., and Schlögl, R., *Catal. Lett.* **60**, 103 (1999).

16. Gao, X., Bañares, M. A., and Wachs, I. E., *J. Catal.* **188**, 325 (1999).

17. Weckhuysen, B. M., Verberckmoes, A. A., Debaere, J., Ooms, K., Langhans, I., and Schoonheydt, R. A., *J. Mol. Catal. A: Chemical* **151**, 115 (2000).

18. Weckhuysen, B. M., and Schoonheydt, R. A., *Catal. Today* **49**, 441 (1999).

19. Deno, N. C., Bollinger, J., Friedman, N., Hafer, K., Hodge, J. D., and Houser, J. J., *J. Am. Chem. Soc.* **85**, 2998 (1963).

20. Olah, G. A., Pittman, C. U. Jr., Waack, R., and Doran, M., *J. Am. Chem. Soc.* **88**, 1488 (1966).

21. Förster, H., Seebode, J., Fejes, P., and Kiricsi, I., *J. Chem. Soc. Faraday Trans. I* **83**, 1109 (1987).

22. Pazé, C., Sazak, B., Zecchina, A., and Dwyer, J., *J. Phys. Chem. B* **103**, 9978 (1999).

23. Brouwer, D. M., in "Chemistry and Chemical Engineering of Catalytic Processes" (R. Prins and G. C. A. Schuit, Eds.), *NATO ASI Ser. E.* **39**, 137 (1980).

24. Suzuki, T., and Okuhara, T., *Chem. Lett.* **5**, 470 (2000).

25. Cheung, T.-K., d'Itri, J. L., and Gates, B. C., *J. Catal.* **151**, 464 (1995).

26. Rezgui, S., and Gates, B. C., *Catal. Lett.* **37**, 5 (1996).

27. Rezgui, S., Jentoft, R.E., and Gates, B.C., *Catal. Lett.* **51**, 229 (1998).

28. Thiede, M., and Melsheimer, J., *Rev. Sci. Inst.* **73**, 394 (2002).

29. Hahn, A., Ressler, T., Jentoft, R.E., and Jentoft, F.C., *Chem. Comm.* 537 (2001).

30. Ciuparu, D., Ensuque, A., Shafeev, G., and Bozon-Verduraz, F., *J. Mater. Sci. Lett.* **19**, 931 (2000).

31. Navío, J. A., Hidalgo, M. C., Colón, G., Botta, S. G., and Litter, M. I., *Langmuir* **17**, 202 (2001).

32. Gutiérrez-Alejandre, A., Ramírez, J., and Busca, G., *Catal. Lett.* **56**, 29 (1998).

33. Kortüm, G., "Reflexionsspektroskopie", Springer-Verlag, Berlin, 1969.

34. Hesse, M., Meier, H., and Zeeh, B., "Spektroskopische Methoden in der Organischen Chemie", Georg Thieme Verlag, Stuttgart, 1984.

35. Luzgin, M. V., Stepanov, A. G., Shmachkova, V. P., and Kotsarenko, N. S., *J. Catal.* **203**, 273 (2001).

36 Tabora, J.E., and Davis, R.J., *J. Am. Chem. Soc.* **118**, 12240 (1996).

37. Greensfelder, B. S., Voge, H. H., and Good, G. M., *Ind. Eng. Chem.* **41**, 2573 (1949).

38. Matsuhashi, H., Shibata, H., Nakamura, H., and Arata, K., *Appl. Catal. A: General* **187**, 99 (1999).

39. Adeeva, V., Lei, G. D., and Sachtler, W. M. H., *Catal. Lett.* **33**, 135 (1995).

List of figures

Figure 9: Rates of formation of isopentane (open pentagons), isobutane (open squares), rate of carbon loss (solid pentagons), and area increase (d[area]/dt) of band at 330 nm (stars) vs. time on stream. Carbon loss is expressed in units of moles C_5. Conditions: 1.29 g SZ; 298 K; 0.25 vol % *n*-pentane in helium; 50 ml min^{-1} total flow at atmospheric pressure.

Figure 1

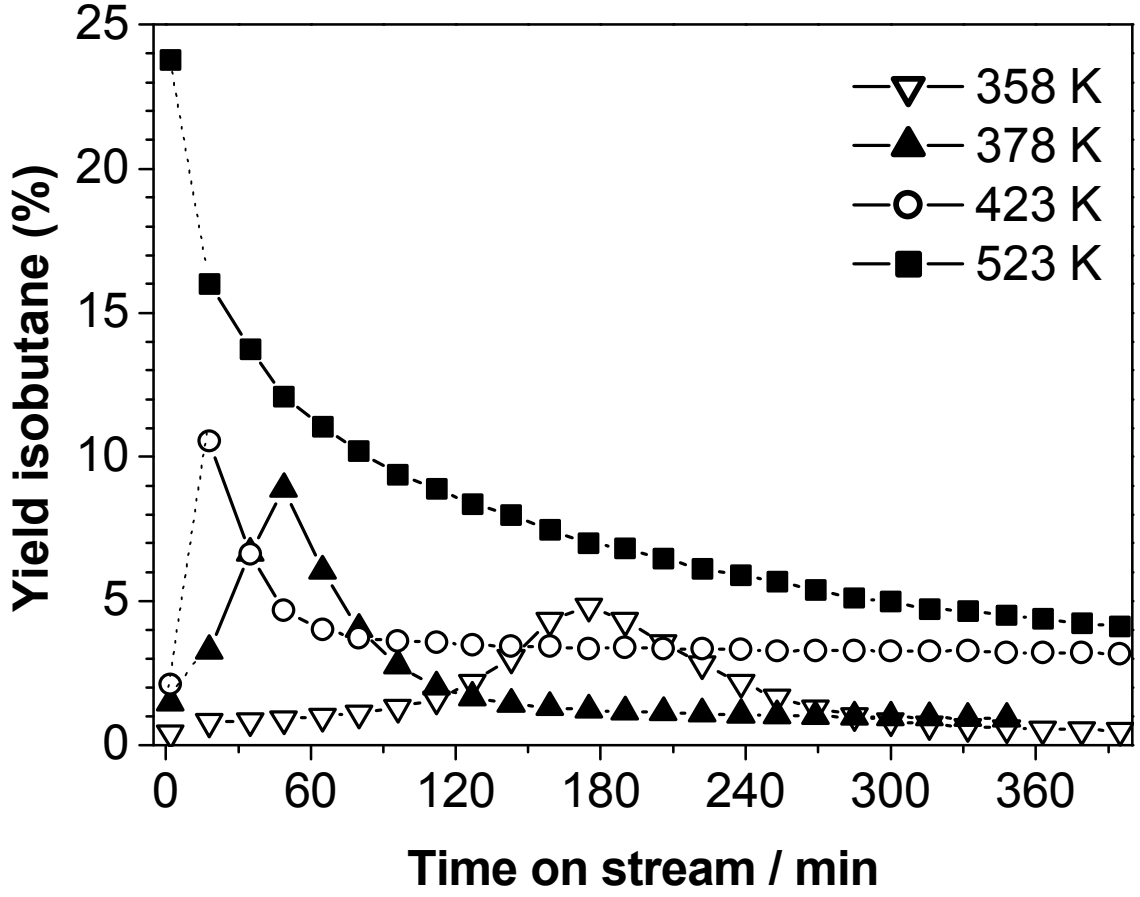
Yield isobutane (%)
Time on stream / min
358 K
378 K
423 K
523 K
0
5
10
15
20
25
0
60
120
180
240
300
360

Figure 2

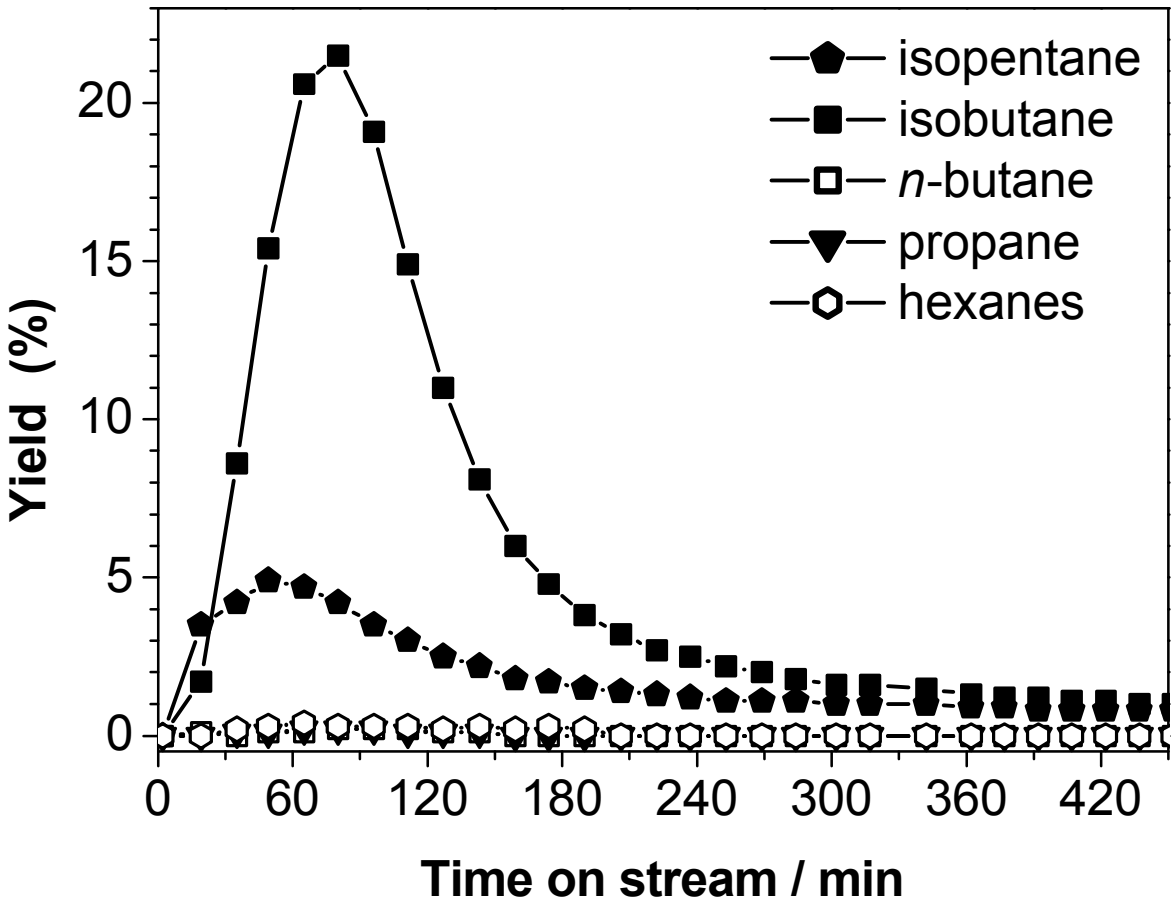
isopentane
isobutane
n-butane
propane
hexanes
Yield (%)
0
5
10
15
20
0
60
120
180
240
300
360
420
Time on stream / min

Figure 3

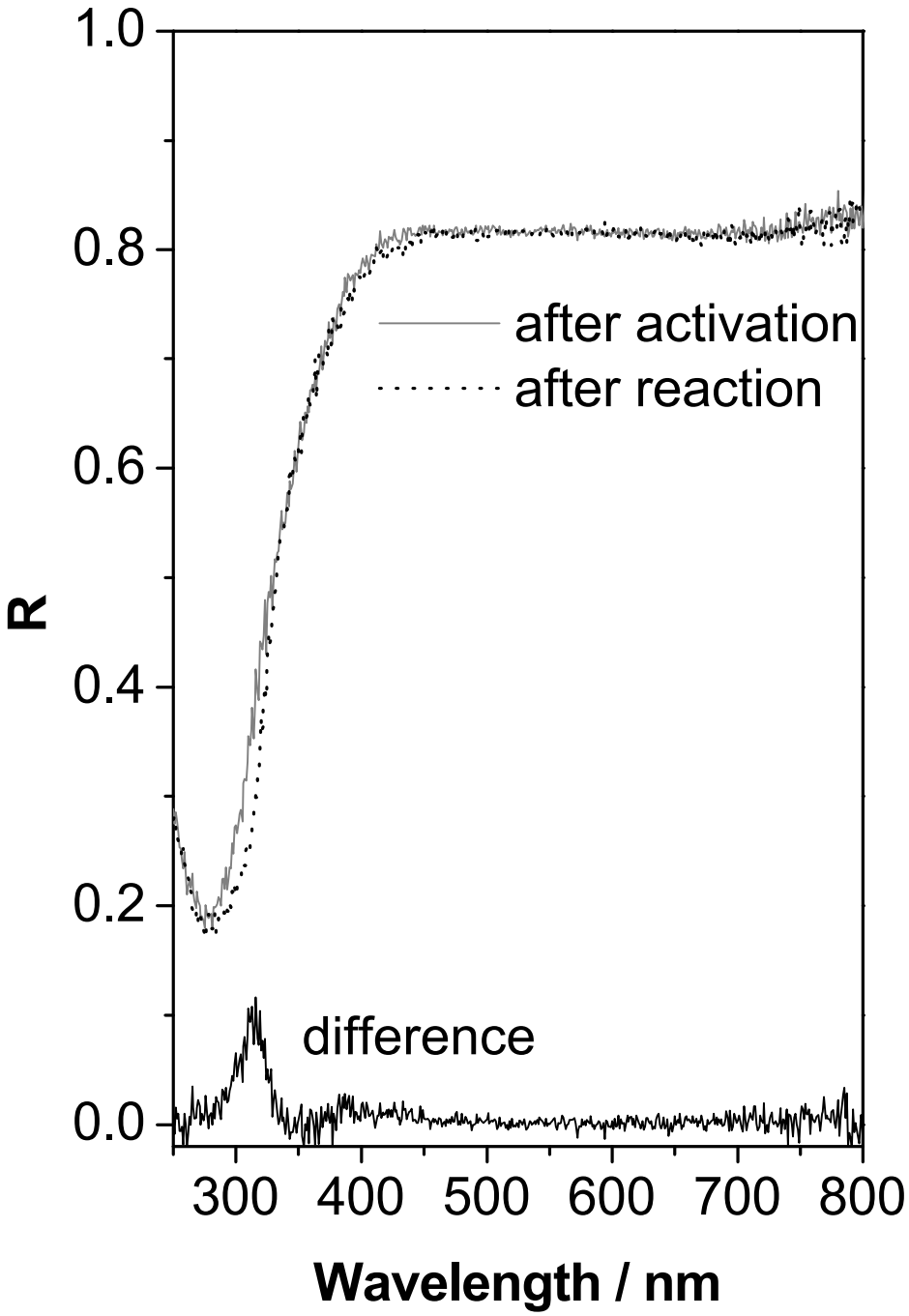
1.0
0.8
0.6
0.4
0.2
0.0
R
after activation
after reaction
difference
300
400
500
600
700
800
Wavelength / nm

Figure 4

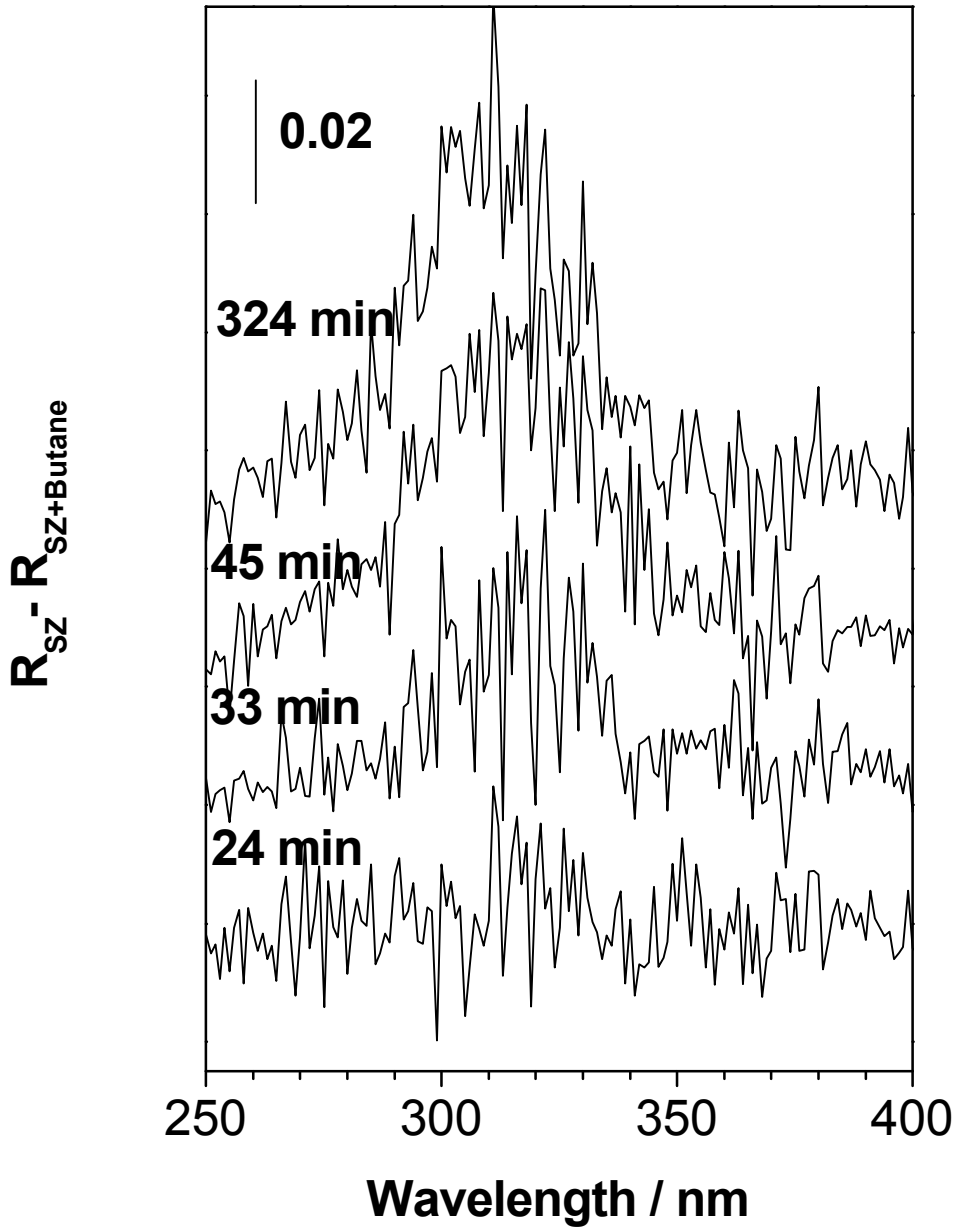
0.02
324 min
45 min
33 min
24 min
$R_{SZ} - R_{SZ+Butane}$
250
300
350
400
Wavelength / nm

Figure 5

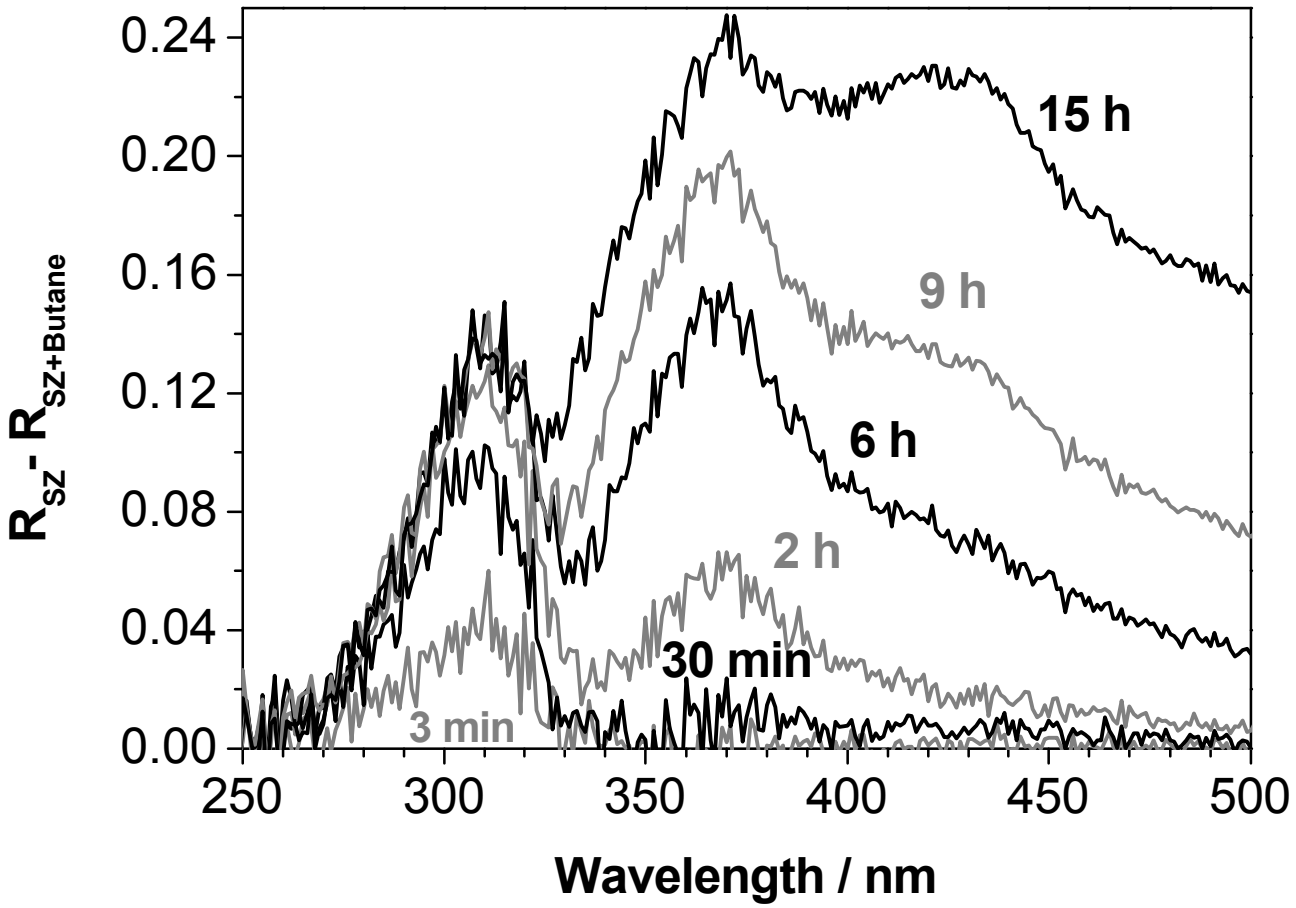
0.24
0.20
0.16
0.12
0.08
0.04
0.00
250
300
350
400
450
500
$R_{SZ} - R_{SZ+Butane}$
Wavelength / nm
15 h
9 h
6 h
2 h
30 min
3 min

Figure 6

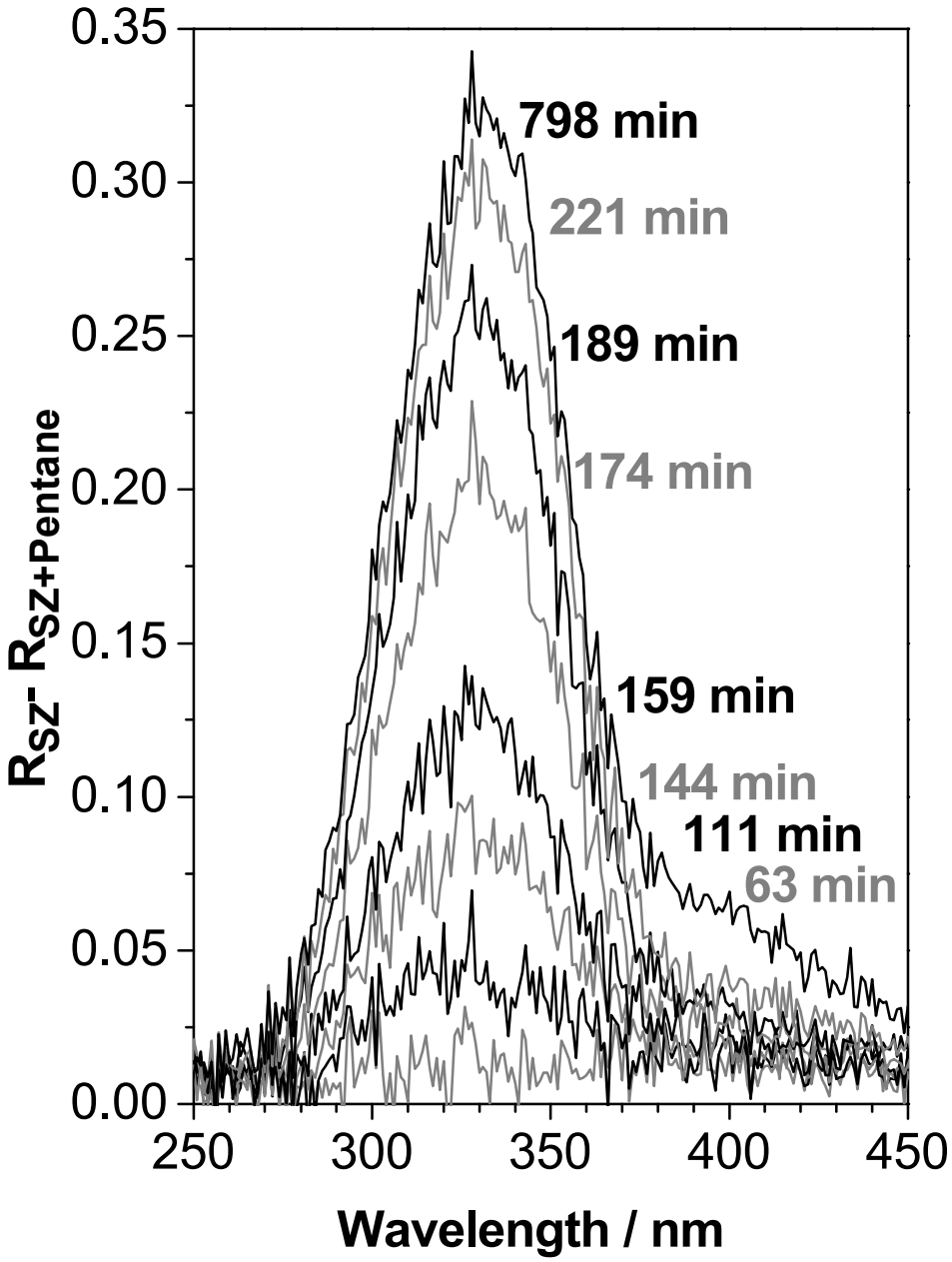
0.35
0.30
0.25
0.20
0.15
0.10
0.05
0.00
250
300
350
400
450
Wavelength / nm
R_SZ- R_SZ+Pentane
798 min
221 min
189 min
174 min
159 min
144 min
111 min
63 min

Figure 7a

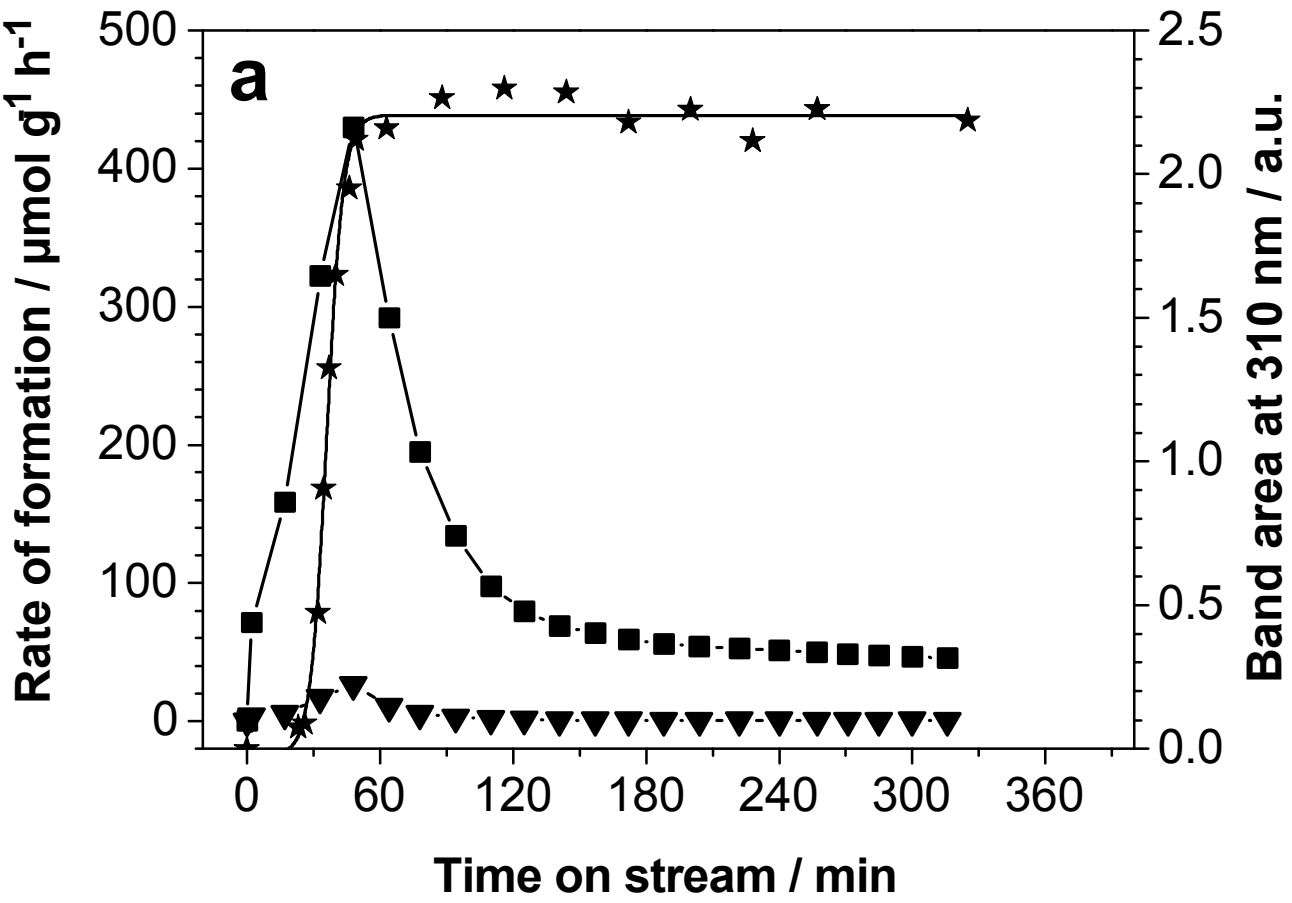
a
Rate of formation / µmol g-1 h-1
Band area at 310 nm / a.u.
Time on stream / min
0
100
200
300
400
500
0.0
0.5
1.0
1.5
2.0
2.5
0
60
120
180
240
300
360

Figure 7b

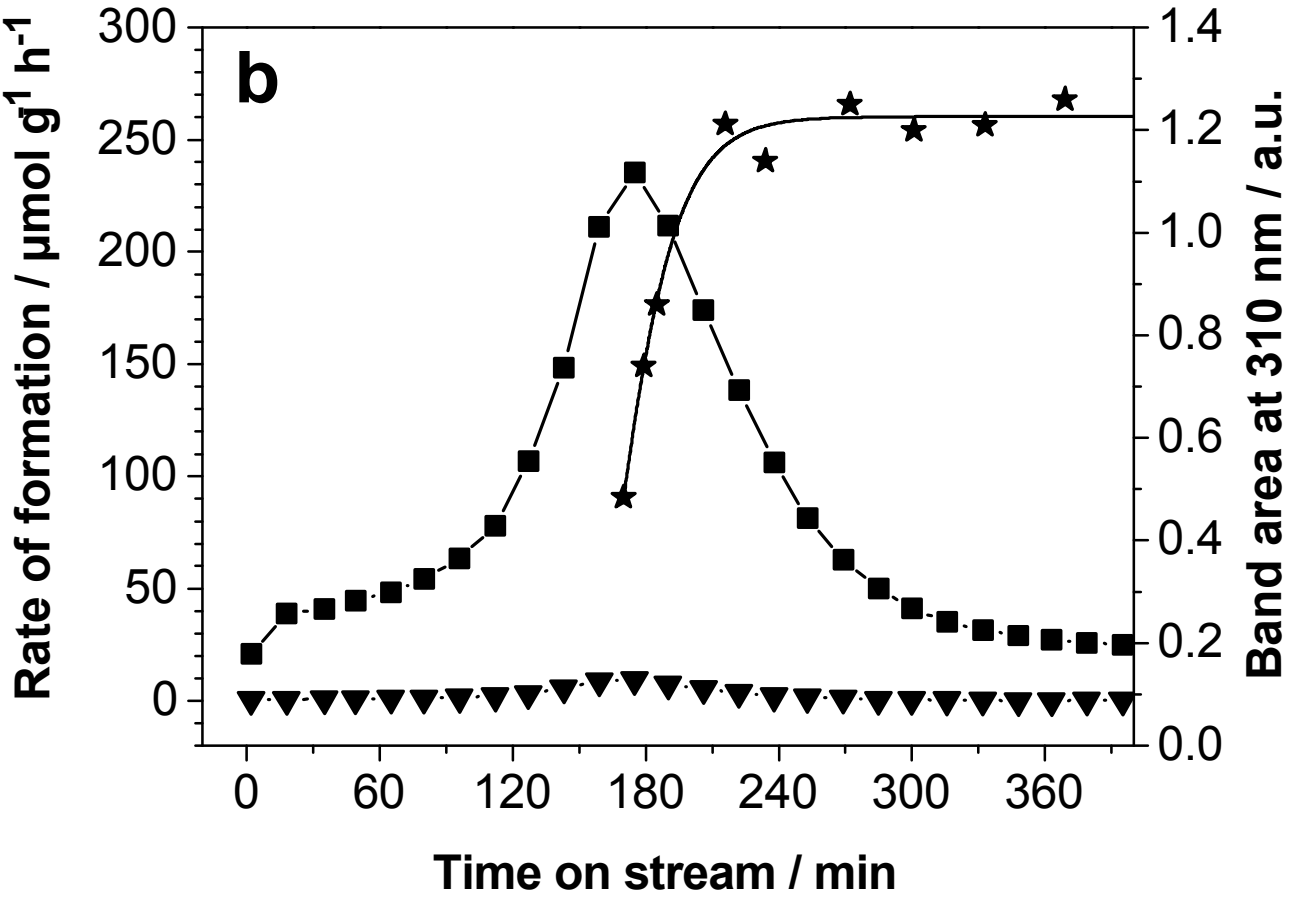
b
Rate of formation / µmol g-1 h-1
Band area at 310 nm / a.u.
Time on stream / min
0
50
100
150
200
250
300
0.0
0.2
0.4
0.6
0.8
1.0
1.2
1.4
0
60
120
180
240
300
360

Figure 8

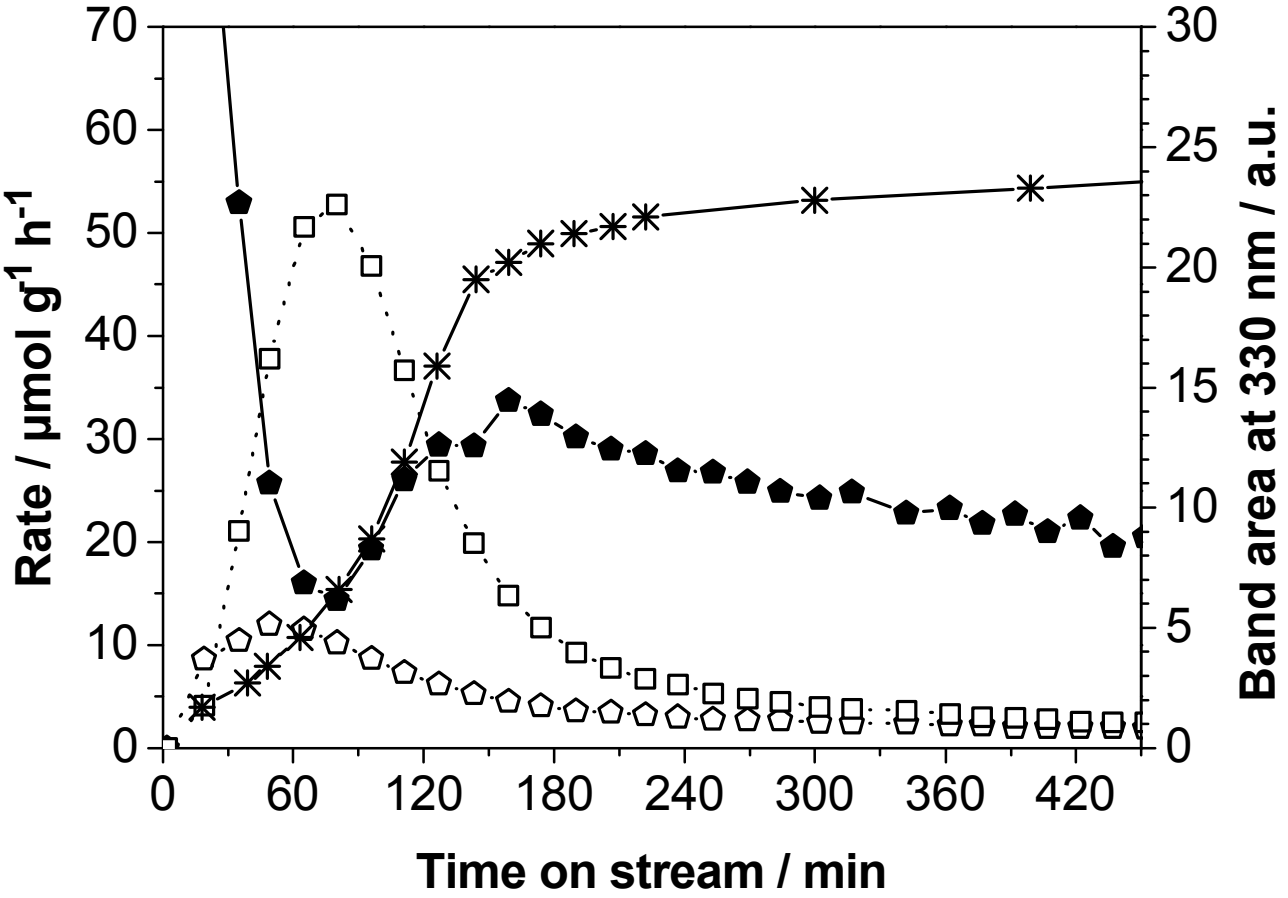
Rate / µmol g-1 h-1
Band area at 330 nm / a.u.
Time on stream / min
0
10
20
30
40
50
60
70
0
5
10
15
20
25
30
0
60
120
180
240
300
360
420

Figure 9

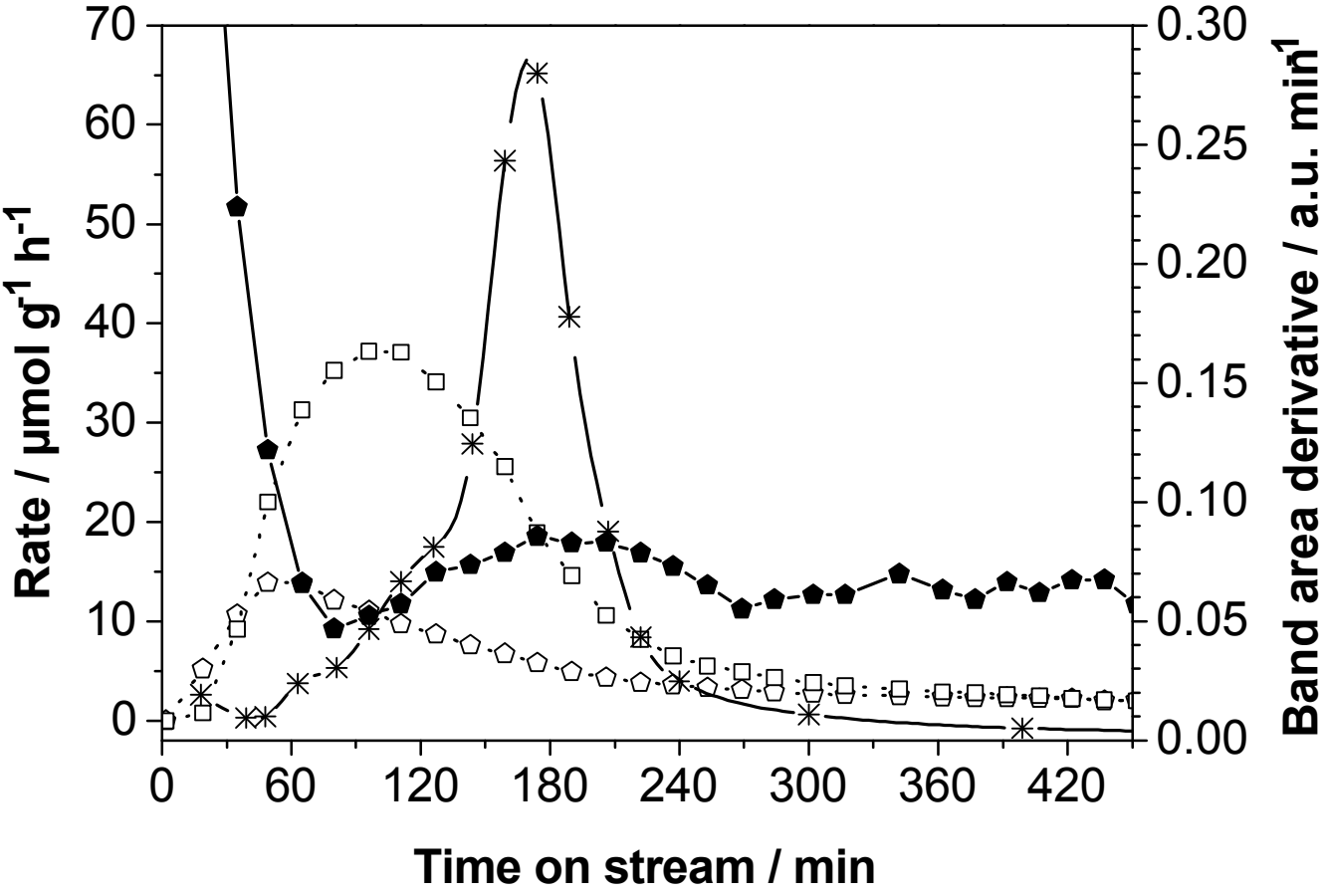
Rate / µmol g-1 h-1
Band area derivative / a.u. min-1
Time on stream / min
0
10
20
30
40
50
60
70
0.00
0.05
0.10
0.15
0.20
0.25
0.30
0
60
120
180
240
300
360
420